AIChE Letter: Particle Technology and Fluidization

A System-Size Independent Validation of CFD-DEM for Noncohesive Particles

Casey Q. LaMarche, Peiyuan Liu, Kevin M. Kellogg, Alan W. Weimer, and Christine M. Hrenya
Dept. of Chemical and Biological Engineering, University of Colorado at Boulder, Boulder, CO 80303

DOI 10.1002/aic.15057
Published online October 5, 2015 in Wiley Online Library (wileyonlinelibrary.com)

Significance
For the first time, CFD-DEM simulations of small-scale fluidized beds are quantitatively validated against large-scale experiments. Such validation is possible via the identification of a measurement independent of system size, namely defluidization. CFD-DEM inputs (particle properties and operating conditions) are measured directly. Sphericity is found to be critical, even for highly spherical particles. This size-independent method of validation is valuable since it allows for validation of CFD-DEM models without restrictions on system sizes or particle sizes. © 2015 American Institute of Chemical Engineers *AIChE J*, 61: 4051–4058, 2015

Keywords: fluidization, CFD-DEM, validation, characterization, size-independent

Introduction

Fluidized beds are known for efficient mixing and contacting, leading to their widespread use for reactions, heat transfer, and mixing. While an empirical understanding has existed for decades, a theoretical understanding is more recently developing.[1] For example, Computational Fluid Dynamics-Discrete Element Method (CFD-DEM)[2] simulations recently provided support for Molerus'[3] theory that Group A particles transition to Group B as cohesive forces are removed.

CFD-DEM is a tool that will continue to be useful in building an enhanced physical picture of the fluidized-bed system. In such simulations, particles are treated as discrete entities via DEM and the fluid is treated as a continuum via CFD. Because each particle is tracked, incorporating particle–particle interactions like collisions is straightforward (i.e., a constitutive relation for collisional stress is not needed), as is the incorporation of additional physics like particle-size distribution, cohesion, etc. However, CFD-DEM is limited to a small number of particles (generally $\lesssim 10^6$), due to high computational overhead,[4] and, thus, simulated systems are generally orders of magnitude smaller than realistic applications ($> 10^8$ particles). Conversely, the Two-Fluid Model (TFM), which treats both gas and solid phases as continuum, is capable of modeling industrial sized systems,[5] but requires constitutive relations (e.g., solid-phase stress) to close the equations of motion. Accordingly, CFD-DEM can be viewed as an "ideal" dataset for validation of TFM since: (1) the tracking of individual particles precludes the need for closures like solid-phase stress, (2) the assumptions of CFD-DEM and TFM can be matched (e.g. smooth particles, perfectly spherical, etc.), and (3) intrusive measurements are avoided. Nonetheless, experimental validation of CFD-DEM is still necessary to instill confidence in the particle–particle interactions (collisions, short-range forces, shape effects, etc.).

In past studies, CFD-DEM predictions were quantitatively compared against numerous experimental measurements that *depend* on system size: particle velocities,[6] voidage,[7] pressure drop and fluctuations,[8] bed expansion,[8,9] and bubble properties;[9,10] see Zhu et al.[11] for a more comprehensive list. For these comparisons, the simulated and experimental system sizes were matched, which restricted the experiments to small apparatuses and large (generally Group D) particles. Specifically, systems were limited to bed-width-to-particle-diameter ratios[6–9] that are small enough for wall effects to make a significant contribution or even dominate results,[12] thereby limiting the ability to conduct a robust validation of practical systems. Furthermore, with validation restricted to large particles, validating the physics that dominates with smaller particles, such as van der Waals forces, is difficult. This restriction of CFD-DEM validation to smaller systems and/or larger particles presents a conundrum when it is used as validation data for TFM models. Namely, the mechanisms at play (e.g., wall effects) may be different in the smaller systems used for validation than in the pilot- and industrial-scale systems of ultimate interest in which TFM will be used. To overcome this obstacle and allow for a robust validation of CFD-DEM at larger scales, a measurement that is *independent* of system size is key.

Unlike previous works, attention here is paid to identifying a measurement that is system-size independent, namely defluidization measurements. Figure 1a illustrates typical fluidization and defluidization curves, or pressure drop across a

Correspondence concerning this article should be addressed to C. M. Hrenya at hrenya@colorado.edu

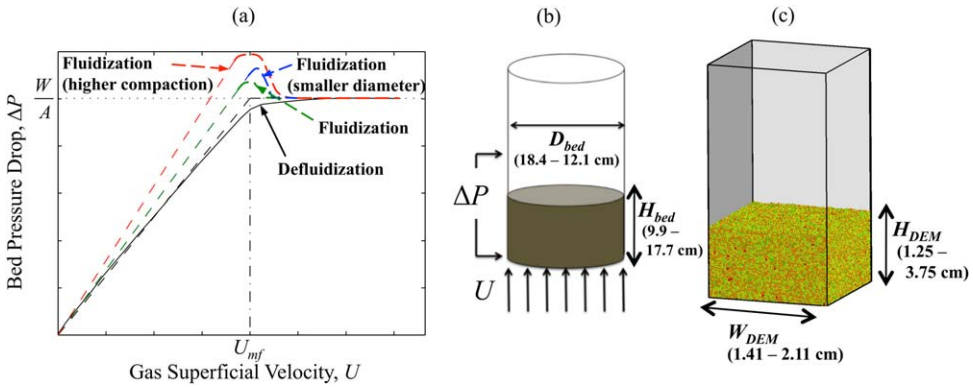

Figure 1. (a) Illustration of fluidization and defluidization curves. Schematic of (b) the experimental system the number of particles is on the order of 10^8, and (c) the CFD-DEM domain where the number of particles is on the order 10^5.

[Color figure can be viewed in the online issue, which is available at wileyonlinelibrary.com.]

particle bed, ΔP, vs. increasing and decreasing superficial gas velocity, U. At lower velocities when particles are stationary, a linear relationship exists between ΔP and U (e.g., dashed black line for $U < U_{\mathrm{mf}}$) which can be described with the Ergun[13] or Carman-Kozeny[14] expressions. When the fluid velocity is sufficiently high for the drag to match the apparent weight of the particle bed, then ΔP remains constant with further increases in U. When fluidized, a macroscopic force balance indicates that ΔP equals the weight of the bed divided by its cross-sectional area (W/A; e.g., horizontal dotted black line in Figure 1a).

The defluidization curve (decreasing U), rather than fluidization (increasing U), is identified for comparison with CFD-DEM because the fluidization branch varies with system size (green and blue dashed lines),[15,16] as depicted in Figure 1a. During fluidization the particles must overcome static friction with the wall to fluidize, and, thus, ΔP overshoots W/A.[15,17] The degree of overshoot depends on system size and will disappear with increasing bed diameter.[17] (A change in the initial packing fraction will also lead to a change in the packed-bed slope during fluidization[16] as shown by red line in Figure 1a, though this effect does not depend on system size.) Conversely, defluidization (solid black line in Figure 1a) is generally insensitive to system size because it does not involve the frictional mechanism just described.[15] Accordingly, the method of Richardson,[18] which utilizes the defluidization curve rather than fluidization, is generally used[19] to determine the minimum fluidization velocity (U_{mf}). Namely, U_{mf} is defined as the velocity at the intersection of the linear, packed-bed region of the defluidization curve (black dashed line), and W/A (horizontal line).[18] Previous studies indicate that, in the presence of particle-wall friction, U_{mf} is independent of domain size above a critical ratio of bed diameter to particle diameter (D_{bed}/d),[20,21] but otherwise U_{mf} increases with decreasing system size.[21,22]

The aim of the current work is twofold: (1) to test the hypothesis that system-size independence of U_{mf} can be achieved in both large-scale experiments and small-scale simulations, and (2) if the hypothesis is supported, demonstrate its applicability to providing a validation of small-scale CFD-DEM with large-scale experiments. An important element of this comparison is carefully measured particle properties (e.g., sphericity, friction) and operating conditions (e.g., humidity), which are used as inputs to the simulations. Such care is needed since U_{mf} is found to be sensitive to particle properties and operating conditions, thereby making U_{mf} a good basis for comparison in validation studies.

Methods

The large discrepancy between the experimental and simulated system size considered here is intentional, for reasons described above. Namely, the bed height (H_{bed}) and diameter (D_{bed}) of the experimental system is $\sim$10 cm (Figure 1b), while the simulated height (H_{DEM}) and width (W_{DEM}) are $\sim$1 cm (Figure 1c). A uniformly distributed stream of air (density 0.97 kg/m^3, and viscosity 1.83×10^{-5} Pa s), which has a controlled velocity, is introduced to the bottom of the bed of particles. The gas velocity is initially high enough ($\sim$ 8 cm/s) to ensure that the bed is fully fluidized, after which the velocity is reduced using small increments. After each reduction, the velocity is held constant long enough to ensure that a stationary state has been reached. The pressure drop across the bed of particles is measured during this stationary state, leading to the defluidization curve.

Experiments—fluidized bed apparatus

The experimental setup is the same apparatus used previously in our group, as detailed elsewhere.[23] Two Plexiglas columns, with diameters of 18.4 cm and 12.0 cm, were used. The incoming air is distributed to the bottom of the column using a 20 μm average porosity sintered 316 stainless steel distributor plate (Mott Corporation). Uniform gas flow was ensured as the pressure drop across the distributor was always greater than 10% of the pressure drop across the bed at U_{mf}.[19] A high initial gas velocity ensured the bed remained bubbling after several velocity reductions. To initialize, the gas was held at the highest velocity for approximately 20 min after the relative humidity of the bed dropped below 3%. The gas velocity was then reduced and held constant for 60 s (60 Hz sampling rate) to ensure that ΔP reached a stationary state; this process was repeated until a zero gas velocity was reached. The resulting defluidization curves from five separate trials were averaged

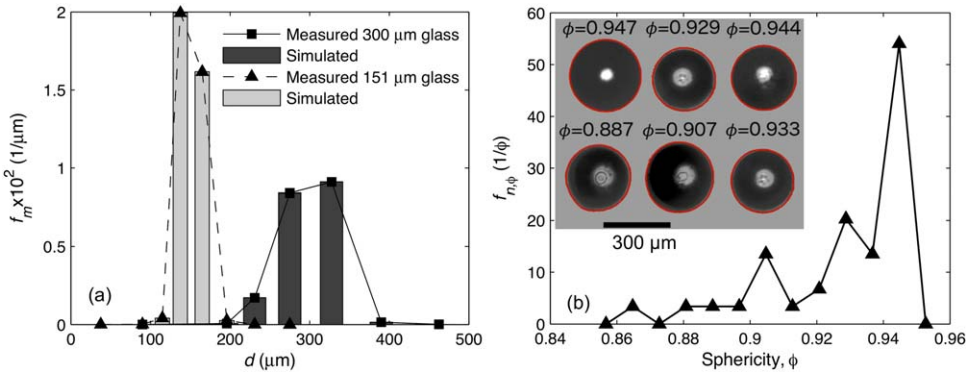

Figure 2. Particle characterization: (a) measured and simulated particle-size distributions (mass-based frequency, f_m) for the 151 and 300 μm glass; (b) sphericity distribution (number-based frequency $f_{n,\phi}$) for 300 μm glass spheres acquired from microscope images with inset of randomly selected examples.

[Color figure can be viewed in the online issue, which is available at wileyonlinelibrary.com.]

and displayed in all defluidization curves, along with 95% confidence intervals.

Precautions were taken to eliminate all sources of cohesion from experiments, for cleanest possible comparison with the (noncohesive) CFD-DEM predictions. To avoid cohesion arising from moisture, a packed silica dryer at the inlet of the fluidized bed controlled the relativity humidity to below 15% for all experiments. The defluidization curves did not change when the relative humidity reduced from 15% to below 3%, indicating humidity is not affecting the results. The humidity was monitored with an Omega HX93AV-RP1 hygrometer under the distributor plate. To minimize electrostatics, antistatic spray (Kensington Dust Guardian) was applied to the walls of the column and a copper wire and metal base were used to ground the system.

A method to estimate the critical ratio of particle to bed diameter, below which the defluidization curve could be system-size dependent, was developed here. The Wen and Yu[24] correlation is widely used for predicting U_{mf}, but the correlation does not include bed size dependence. Conversely, Rao et al.[25] adjusted the Wen and Yu correlation to include bed size dependence. However, the Rao et al.[25] correlation does not predicts a critical bed size needed for bed-size independence (i.e., it asymptotes to the Wen and Yu[24] correlation, incorrectly indicating a bed would need to be infinitely large). Thus, the Rao et al.[25] and Wen and Yu[24] correlations are combined to approximate the critical bed diameter for our system. In particular, the critical bed diameter is defined as the diameter when the Rao et al.[25] correlation for U_{mf} is within 0.5% of the value obtained from Wen and Yu.[24] Using this method, the critical bed diameters are found to be approximately 500d and 400d for the smaller and larger particles studied here, respectively; both are well below the sizes of the experimental system.

Particle characterization

The spherical soda-lime glass particles, acquired from Mo-Sci, are Geldart Group B and, thus, van der Waals forces are negligible.[3] Two particle size ranges were investigated, both relatively monodisperse, with arithmetic mean diameters, d_{ave}, of 151 μm and 300 μm. For simplicity, the former and latter particle size ranges are referred to as 151 μm glass and 300 μm glass, respectively. The Sauter mean diameters for the two particles, calculated based on an assumption of spherical particles, are similar to the arithmetic mass mean, namely 150 μm and 296 μm (Sauter means) for the 151 μm and 300 μm glass (arithmetic means), respectively. Particle-size distributions were measured via careful and repeatable sieving, and the distributions are provided in Figure 2a. The distribution of particle sizes within a given bin (sieve) is unknown; the black lines between measured frequencies are used to express such a continuum of particle sizes. While both particle size ranges are relatively monodisperse, they are made up of a narrow distribution of particle sizes. When considering the full particle-size distribution, simulations are called polydisperse; similarly, monodisperse is used to refer to the case of simulating particles of a single size (d_{ave}).

Sphericity, ϕ, is a measurement of particle shape and is classically defined as the ratio of the surface area of a sphere with the equivalent volume of the particle to the surface area of the particle,[26] but can be estimated accurately from two-dimensional images.[27] Here, the ratio of the equivalent-sphere, projected-area diameter to the equivalent-sphere, projected-perimeter diameter is used to measure ϕ[28] via optical microscopy. The sphericity value is based on the macroscopic perimeter measurement (i.e., deviation of the perimeter from a circle with the same area), and is not a measurement of microscopic roughness. Figure 2b contains the number-based frequency distribution of ϕ ($f_{n,\phi}$) measurements for the 300 μm glass spheres. Similar to the particle-size distribution in Figure 2a, $f_{n,\phi}$ in Figure 2b is a discrete representation of a continuous value. The microscope images were analyzed using image-processing software written in MATLAB. First, images are segmented using the thresholding method, which uses the pixel intensities to convert a grayscale image to binary (black and white). The inset of Figure 2b provides original particle images (randomly selected), along with the tracked outlines in red. The perimeter and area of identified particles were used to calculate the sphericity. The resulting values of mean sphericity for the 300 μm and 151 μm glass particles are 0.93 and 0.94, respectively. It is worthwhile to note that the particles

Table 1. Parameters Used in Simulations

Parameter	Value
Mean particle diameter, d_{ave} (μm)	151 and 300
Particle intrinsic density, ρ_p (kg/m^3)	2500
Particle–particle friction coefficient, μ	0.275, 0.1, 0.4
Normal coefficient of restitution, e	0.97
Total number of particles	117,299–351,897
Base case static bed geometry (300 μm glass) (cm)	$H_{DEM} = 1.25$, $W_{DEM} = 1.41$
Varied static bed geometries (300 μm glass) (cm)	$H_{DEM} = 1.25$–3.75, $W_{DEM} = 1.41$–2.11
Static bed geometry (151 μm glass) (cm)	$H_{DEM} = 0.59$, $W_{DEM} = 0.71$
Gas density, ρ_g (kg/m^3)	0.97
Gas viscosity, μ_g (Pa s)	1.8335×10^{-5}

appear spherical via a visual inspection of the particle in the inset of Figure 2b, though the measured values reveal a slight nonsphericity not easily perceived by the eye.

The friction coefficient was measured using 2 mm soda-lime glass spheres from the same manufacturer, by measuring the acceleration of sleds (constructed by epoxying the spheres to the bottom four corners of glass microscope cover slips) down glass plates with known inclination angles. The measured kinetic particle–particle friction coefficient, $\mu = 0.273 \pm 0.02$, was measured at a relative humidity below 5%. The coefficient of restitution reported in the literature for glass, $e = 0.97$.[29] This value was confirmed via imaging measurements of precollision and postcollision velocities from a few drop experiments of 2 mm glass spheres on a glass surface.

CFD-DEM simulations

The CFD-DEM simulations were conducted using the open-source code MFIX (Multiphase Flow with Interphase eXchange).[30] A brief summary of the simulations is provided below, with more details available elsewhere.[31]

CFD-DEM governing equations

Details of the CFD fluid solver can be found in the MFIX theory manual[30] and user guide. For DEM, the solids phase is treated as discrete, cohesionless particles. For particle of mass m, and rotational velocity, $\boldsymbol{\omega}_s$, are solved by Newton's equations of motion

$$m\frac{d\mathbf{u_s}}{dt} = \mathbf{f_c} + \mathbf{f_f} + m\mathbf{g} \tag{1}$$

$$I\frac{d\boldsymbol{\omega}_s}{dt} = \mathbf{T} \tag{2}$$

where $\mathbf{g}$ is the acceleration due to gravity, $\mathbf{T}$ is the torque due to the tangential component of the contact force, and I is the moment of inertia. Additionally, $\mathbf{f_c}$ is the contact force due to particle–particle and particle-wall contacts and is given by the visco-elastic contact models of Tsuji et al.[32] and Antypov and Elliott.[33] The fluid-particle interaction, $\mathbf{f_f}$, associated with particle i is given by

$$\mathbf{f_f^i} = -V_i\nabla P_g - \frac{V_i\beta}{1\text{-}\varepsilon}(\mathbf{u_g}-\mathbf{u_s}) \tag{3}$$

where V_i is the volume of the particle, P_g is the gas pressure, β is the gas–solid frictional coefficient, $\mathbf{u_s}$ is the translational particle velocity, $\mathbf{u_g}$ is the gas velocity, and ε is the porosity. β can be obtained from different drag models, with the general form given by van der Hoef et al.[34]

$$\beta = 18\mu_g\,\varepsilon^2(1-\varepsilon)\frac{F}{d_{s,eq}^2} \tag{4}$$

where F is a nondimensional drag force, and is a function of Reynolds number and solids volume fraction. The Koch–Hill drag force model was used in this study; the detailed expression of F can be found in Benyahia et al.[35] To account for the particle shape, an equivalent-spherical particle diameter, $d_{s,eq}$, is used in the drag law by multiplying the sphericity with the particle diameter,[36] d, as $d_{s,eq} = \phi d$. The particle shape is only accounted for in the drag force, as the particles used here are close enough to perfect spheres such that the slight nonsphericity is expected have a negligible impact on particle contact detection and subsequent dynamics. It is also worth noting that the Koch–Hill[35] model is based on DNS simulations of cohesionless spheres, making it more analogous to the conditions of the current study (experiments and CFD-DEM) than the more common empirical drag models.[24,37] Specifically, experiments were controlled to reduce cohesion to negligible levels (humidity and electrostatics) and particles as close to spherical as possible were used. For these reasons, the Koch–Hill drag model showed better agreement with experiments than the Gidaspow[37] and Wen and Yu[24] drag correlations (results not shown for the sake of brevity).

Simulation conditions

CFD-DEM simulations were performed in a 3-D rectangular fluidized bed, as illustrated in Figure 1c. To initialize the bed for the defluidization simulations, particles settled into a static packing, in the absence of gas flow. Next, a gas velocity high enough to ensure a fully fluidized (~5–8 cm/s) bed was initiated. Each subsequent, reduced gas velocity was held constant for 0.1 s, which provided sufficient time for the pressure drop across the bed to become stationary. After reaching stationary state, the pressure drop time series (sampled at 200 Hz) was used for the average and 95% confidence intervals displayed in all defluidization curves. The simulations and experiments provide consistent observations on the fluidization behavior upon defluidization, specifically that the bed is bubbling until U_{mf} is reached and then settles into a packed bed.

Wall effects are minimized by simulating frictionless walls for the particles and free slip (zero velocity gradient) for the gas, in order to mimic a system with a much larger diameter, as in the experiment. No sensitivity was predicted to increasing the bed width and static bed height (via a corresponding increase in the number of particles simulated; see Table 1), ensuring insensitivity to domain size. The simulated ($O(10^5)$ particles) and experimental ($O(10^8)$ particles) systems intentionally are on different scales. The CFD grid size was set to twice the maximum particle diameter in the system, and no sensitivity was found when the grid size was increased to four times the maximum particle size. Table 1 summarizes the properties of solid and gas phases used in CFD-DEM simulations.

The defluidization curve was confirmed to be independent of Young's modulus (E) for the particles studied here, where U_{mf} deviated by less than 0.53% for E ranging from 10 MPa

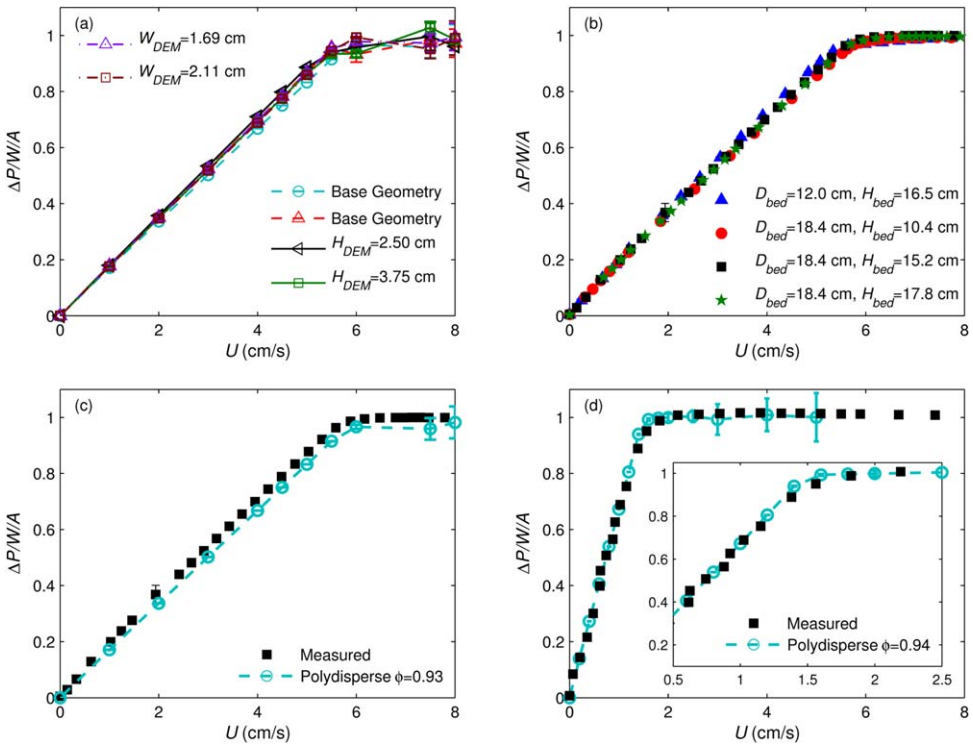

Figure 3. Defluidization curves: independence of system size for 300 μm glass in (a) CFD-DEM predictions (polydisperse, $\phi = 0.93$) and (b) experiments. Qualitative and quantitative agreement between measured and CFD-DEM predictions of (c) 300 μm and (d) 151 μm glass.

Error bars for experiments and simulations represent 95% confidence intervals; error bars are often too small to distinguish on scale of plot. [Color figure can be viewed in the online issue, which is available at wileyonlinelibrary.com.]

to 73000 MPa (results are not shown for the sake of brevity). As the time step is proportional to $E^{-0.4}$, implementing a much softer Young's modulus (100 MPa) than the realistic value (73,000 MPa) reduced computational cost without sacrificing physical accuracy.[4,38,39]

Results and Discussion

In this section, the measured and predicted defluidization curves are compared. First, the independence of the defluidization curve on system size is verified for both the experiments and simulations. Next, quantitative agreement is presented when incorporating measured particle properties and operating conditions. Finally, a sensitivity of predictions to particle shape, friction, and size distribution is discussed.

To test the hypothesis that the defluidization is system-size independent, simulations and experiments were performed with varied bed sizes, as shown in Figures 3a, b, respectively. In Figure 3a, the legend indicates the dimension (H_{DEM} or W_{DEM}) that is varied from the base value (see Table 1). CFD-DEM simulations of varied bed sizes display small variation in the defluidization curves, which is traced to differences in initial conditions of the beds rather than wall effects, as particle-based systems are known to exhibit fluctuations in packing densities.[40] The bed diameters used in our experiments are large enough to ensure that such dependencies are eliminated. Specifically, a repetition of the base geometry with different initial particle placements resulted in a change of U_{mf} from 5.58 cm/s to 5.85 cm/s (relative difference of 5%). The predicted U_{mf} values from all geometries investigated lie within this range, except for $H_{\mathrm{DEM}} = 2.5$ cm and $W_{\mathrm{DEM}} = 1.41$ cm, where $U_{\mathrm{mf}} = 5.53$ cm/s is just slightly outside this range. In Figure 3b, the experimental system is shown to be insensitive to bed height and diameter, which is in agreement with previous observations[20] for similar particle sizes in smaller diameter beds. The independence of experiments on column diameter indicates wall effects (e.g., particle-wall friction) are negligible and allows for a consistent comparison to simulations, which employ frictionless walls.

Given the independence of the defluidization curve to system size in both simulations and experiments (Figures 3a, b), the simulation of the small-scale fluidized bed is compared to measurements from the large-scale experiments in Figures 3c, d. Quantitative agreement is possible only when (1) using carefully measured particle properties (e.g., sphericity) rather than estimates from tabulated values, and (2) eliminating any mechanism from the experiments that was not modeled (e.g., relative humidity or static effects). For the 150 μm glass (Figure 3d), the measured (1.53 ± 0.09 cm/s) and predicted (1.48 cm/s) U_{mf} values are in excellent agreement. Similarly, for the 300 μm glass (Figure 3c) agreement is found between measured $U_{\mathrm{mf}} = 5.56 \pm 0.06$ cm/s, and predicted $U_{\mathrm{mf}} = 5.67 \pm 0.13$ cm/s, which considers all system sizes investigated via averaging of all trials at all bed sizes. In Figure 3c,

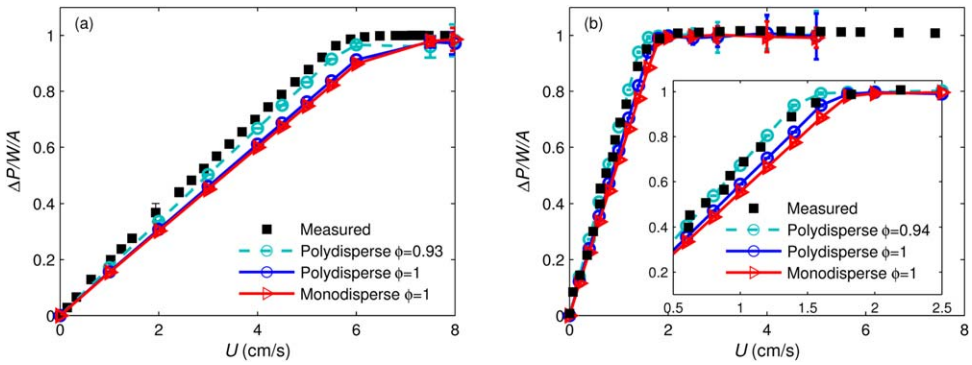

Figure 4. Defluidization curves: measured and CFD-DEM predictions investigating effects of particle shape and polydispersity for (a) 300 μm and (b) 151 μm glass.

Error bars for experiments and simulations represent 95% confidence intervals; error bars are often too small to distinguish on scale of plot. [Color figure can be viewed in the online issue, which is available at wileyonlinelibrary.com.]

only the base geometries for the measured ($D_{bed} = 18.4$ cm, $H_{bed} = 15.2$ cm) and simulated defluidization curves are plotted due to the overlapping agreement of the various sizes (Figures 3a, b). Furthermore, the CFD-DEM predictions are more quantitatively accurate for predicting U_{mf} (2–3.3% error) than classic correlations[24,41] (17–21% error when assuming spherical particles and 6–16% error when including the measured sphericity).

As mentioned previously, careful characterization of particles used in experiments is critical for a successful simulation-experimental comparison. Figure 4 demonstrates the sensitivity of CFD-DEM predictions to particle shape and size distribution for two different particles sizes. For the narrow particle-size distributions studied in this work, monodisperse simulations using the arithmetic-mean particle diameters (red lines with triangles) are good approximations of the true distributions (blue lines with circles). However, when considering perfect spheres ($\phi = 1$), neither the monodisperse or polydisperse predictions quantitatively agree with the measured defluidization curve (black squares). For accurate, quantitative prediction of the defluidization curve, accounting for the slight nonsphericity ($\phi = 0.93$–0.94; cyan dashed line) of the particles is necessary. Particle shape is only accounted for in the drag model of the CFD-DEM, as explained above. Inclusion of this shape effect increases the drag force (Eq. 4), resulting in a smaller U_{mf}. Accounting for the nonspherical nature enhances the relative change of U_{mf} in the smaller particle (13% difference; Figure 4b) compared to the larger (10% difference; Figure 4a). The increased sensitivity of the smaller glass particles is due to the nonlinear dependence of drag on particle diameter. Li et al.[42] is one of the few studies to perform a sensitivity test to particle shape in fluidization CFD-DEM, specifically on voidage and particle velocity profiles in bubbling beds. They predict an increase in voidage and particle velocities when accounting for shape, which they also attribute to increased drag force. It is worth noting that the effect of shape, Figure 4, is more significant than the sensitivity to initial condition explained with respect to Figures 3a, b.

The defluidization curve also exhibits sensitivity to the particle–particle friction, similar to the predictions of Galvin and Benyahia[43] for cohesive particles. Specifically, friction coefficients of $\mu = 0.1$ and 0.4 resulted in predicted U_{mf} values differing by more than 8% from the U_{mf} predicted when using the measured value of $\mu = 0.275$ (results not shown for sake of brevity), indicating that accurate prediction of the defluidization curve relies on implementing the measured friction coefficient. CFD-DEM predictions are only marginally sensitive to the range of coefficient of restitutions investigated ($e = 0.6$ to 0.97; results not shown for sake of brevity).

Concluding Remarks

The overarching contribution of this work is the ability to quantitatively validate small-scale CFD-DEM simulations with large-scale experiments via the identification of a system-size independent measurement—the defluidization velocity. Careful measurement of material properties such as particle size, friction, and shape are necessary for accurate predictions. In particular, to achieve quantitative agreement within the experimental error, the nonspherical shape of particles must be measured and incorporated into simulations. Even for highly spherical particles ($\phi \geq 0.93$), which look like spheres to the eye, accounting for nonsphericities is necessary. Additionally, care must be taken to minimize experimental effects that are not included in the model such as cohesion (i.e., van der Waals, relative humidity and electrostatics). Accordingly, this work demonstrates that the defluidization curve provides a nontrivial validation due to the measurable sensitivity of U_{mf} to material properties and system conditions.

The identification of a system-size independent measurement provides a new avenue for validating physical models in CFD-DEM without being constrained to a small experimental apparatus and/or large particles, which may favor mechanisms not present at larger scales (e.g., wall effects) and, thus, preclude a robust validation. Examples of physical models that can be tested using this methodology include the effects of cohesion (van der Waals, liquid bridging, etc.), particle shape, and particle breakage. Once these physical models are validated, CFD-DEM can be used with confidence to build and test constitutive relations for two-fluid (continuum) models without the need to rely on empiricism or adjustable parameters.

Acknowledgments

The authors thank Dow Corning Corporation for providing funding for this work. This work utilized the Janus supercomputer, which is

supported by the National Science Foundation (award number CNS-0821794) and the University of Colorado Boulder. The Janus supercomputer is a joint effort of the University of Colorado Boulder, the University of Colorado Denver and the National Center for Atmospheric Research. Janus is operated by the University of Colorado Boulder. The authors also thank Kacey Paulin and Andrew Miller for their contributions in setting up experiments, and Kyle Berger for insightful conversations on this work.

Literature Cited

1. van der Hoef MA, van Sint Annaland M, Deen NG, Kuipers JAM. Numerical simulation of dense gas-solid fluidized beds: a multiscale modeling strategy. *Annu Rev Fluid Mech*. 2008;40(1):47–70.
2. Hou QF, Zhou ZY, Yu AB. Micromechanical modeling and anaylsis of different flow regimes in gas fluidization. *Chem Eng Sci*. 2012;84:449–468.
3. Molerus O. Interpretation of Geldart's type A, B, C and D powders by taking into account interparticle cohesion forces. *Powder Technol*. 1982;33(1):81–87.
4. Liu P, Hrenya CM. Challenges of DEM: I. Competing bottlenecks in parallelization of gas–solid flows. *Powder Technol*. 2014;264:620–626.
5. Curtis JS, van Wachem B. Modeling particle-laden flows: a research outlook. *AIChE J*. 2004;50(11):2638–2645.
6. Müller CR, Holland DJ, Sederman AJ, Scott SA, Dennis JS, Gladden LF. Granular temperature: comparison of magnetic resonance measurements with discrete element model simulations. *Powder Technol*. 2008;184(2):241–253.
7. Müller CR, Scott SA, Holland DJ, Clarke BC, Sederman AJ, Dennis JS, Gladden LF. Validation of a discrete element model using magnetic resonance measurements. *Particuology*. 2009;7(4):297–306.
8. Alobaid F, Epple B. Improvement, validation and application of CFD/DEM model to dense gas–solid flow in a fluidized bed. *Particuology*. 2013;11(5):514–526.
9. Van Wachem B, Van der Schaaf J, Schouten JC, Krishna R, van den Bleek CM. Experimental validation of Lagrangian–Eulerian simulations of fluidized beds. *Powder Technol*. 2001;116(2):155–165.
10. Kobayashi T, Tanaka T, Shimada N, Kawaguchi T. DEM–CFD analysis of fluidization behavior of Geldart Group A particles using a dynamic adhesion force model. *Powder Technol*. 2013;248:143–152.
11. Zhu HP, Zhou ZY, Yang RY, Yu AB. Discrete particle simulation of particulate systems: a review of major applications and findings. *Chem Eng Sci*. 2008;63(23):5728–5770.
12. Li T, Gopalakrishnan P, Garg R, Shahnam M. CFD–DEM study of effect of bed thickness for bubbling fluidized beds. *Particuology*. 2012;10(5):532–541.
13. Ergun S. Fluid flow through packed columns. *Chem Eng Prog*. 1952;48:89–94.
14. Carman PC. Fluid flow through granular beds. *Trans Inst Chem Eng*. 1937;15:150–166.
15. Tsinontides SC, Jackson R. The mechanics of gas fluidized beds with an interval of stable fluidization. *J Fluid Mech*. 1993;255:237–274.
16. Yang WC. *Handbook of Fluidization and Fluid-Particle Systems*. New York: CRC Press, 2003.
17. Loezos PN, Costamagna P, Sundaresan S. The role of contact stresses and wall friction on fluidization. *Chem Eng Sci*. 2002;57(24):5123–5141.
18. Richardson JF. Incipient fluidization and particulate systems. In: Davidson JF, Harrison D, editors. *Fluidization*. New York: American Press, 1971:25–64.
19. Kunii D, Levenspiel O. *Fluidization Engineering*, 2nd ed. Boston: Butterworth-Heinemann, 1991.
20. Liu X, Xu G, Gao S. Micro fluidized beds: wall effect and operability. *Chem Eng J*. 2008;137(2):302–307.
21. Kathuria DG, Saxena SC. A variable-thickness two-dimensional bed for investigating gas—solid fluidized bed hydrodynamics. *Powder Technol*. 1987;53(2):91–96.
22. Rowe PN, Everett DJ. Fluidised bed bubbles viewed by X-rays part II - The transition from two to three dimensions of undisturbed bubbles. *Trans Inst Chem Eng*. 1972;50(1):42–48.
23. Joseph GG, Leboreiro J, Hrenya CM, Stevens AR. Experimental segregation profiles in bubbling gas-fluidized beds. *AIChE J*. 2007;53(11):2804–2813.
24. Wen C, Yu YH. Mechanics of fluidization. *Chem Eng Prog Symp Ser*. 1966;62(62):100–111.
25. Rao A, Curtis JS, Hancock BC, Wassgren C. The effect of column diameter and bed height on minimum fluidization velocity. *AIChE J*. 2010;56(9):2304–2311.
26. Wadell H. Sphericity and roundness of rock particles. *J Geol*. 1933; 41(3):310–331.
27. Cavarretta I, O'Sullivan C, Coop MR. Applying 2D shape analysis techniques to granular materials with 3D particle geometries. *AIP Conf Proc*. 2009;1145(1):833–836.
28. *International Organization for Standardization*. ISO I. 9276–6: 2008. *International Organization for Standardization, Geneva*. 2008.
29. Foerster SF, Louge MY, Chang H, Allia K. Measurements of the collision properties of small spheres. *Phys Fluids*. 1994;6(3):1108.
30. Syamlal M, Rogers W, O'Brien TJ. *MFIX Documentation: Theory Guide*, Technical Note, DOE/METC-94/1004, NTIS/DE94000087, Springfield, VA: National Technical Information Service, 1993.
31. Liu P, LaMarche CQ, Kellogg KM, Hrenya CM. Defluidization of cohesive particles: interaction between cohesion, Young's modulus and static bed height. *Phys Rev E*. Submitted.
32. Tsuji Y, Tanaka T, Ishida T. Lagrangian numerical simulation of plug flow of cohesionless particles in a horizontal pipe. *Powder Technol*. 1992;71(3):239–250.
33. Antypov D, Elliott JA. On an analytical solution for the damped Hertzian spring. *Europhysics Lett (EPL)*. 2011;94(5):50004.
34. van der Hoef MA, Beetstra R, Kuipers JAM. Lattice-Boltzmann simulations of low-Reynolds-number flow past mono- and bidisperse arrays of spheres: results for the permeability and drag force. *J Fluid Mech*. 2005;528:233–254.
35. Benyahia S, Syamlal M, O'Brien TJ. Extension of Hill–Koch–Ladd drag correlation over all ranges of Reynolds

number and solids volume fraction. *Powder Technol.* 2006;162(2):166–174.
36. Kunii D, Levenspiel O. Circulating fluidized-bed reactors. *Chem Eng Sci.* 1997;52(15):2471–2482.
37. Gidaspow D. *Multiphase Flow and Fluidization*. Boston: Academic Press, 1994.
38. Moreno-Atanasio R, Xu BH, Ghadiri M. Computer simulation of the effect of contact stiffness and adhesion on the fluidization behaviour of powders. *Chem Eng Sci.* 2007;62(1–2): 184–194.
39. Mikami T, Kamiya H, Horio M. Numerical simulation of cohesive powder behavior in a fluidized bed. *Chem Eng Sci.* 1998;53(10):1927–1940.
40. Nowak ER, Knight JB, Ben-Naim E, Jaeger HM, Nagel SR. Density fluctuations in vibrated granular materials. *Phys Rev E.* 1998;57(2):1971.
41. Chen JJJ. Comments on "improved equation for the calculation of minimum fluidization velocity." *Ind Eng Chem Res.* 1987;26:633–634.
42. Li T, Garg R, Galvin J, Pannala S. Open-source MFIX-DEM software for gas-solids flows: Part II—Validation studies. *Powder Technol.* 2012;220:138–150.
43. Galvin JE, Benyahia S. The effect of cohesive forces on the fluidization of aeratable powders. *AIChE J.* 2014; 60(2):473–484.

Manuscript received June 18, 2015.